Neutron-scattering and electron-microscopy studies of the premartensitic phenomena in Ni_xAl_{100-x} alloys

S. M. Shapiro and B. X. Yang*
Brookhaven National Laboratory, Upton, New York 11973

Y. Noda
Chiba University, Yayoi, Chiba, 260 Japan

L. E. Tanner and D. Schryvers†
Lawrence Livermore National Laboratory, Livermore, California 94550

(Received 17 April 1991)

Inelastic-neutron-scattering and electron-microscopy studies were performed on single crystals of the cubic phase of Ni_xAl_{100-x} alloys for $x=50$, 58, 62.5, and 63.9 at. %. The [110]-TA_2 phonon branch, corresponding to atomic displacements along the $[\bar{1}10]$ direction, is shown to exhibit anomalous behavior in that the entire branch is very sensitive to composition and exhibits a "kink" whose position in q space is also sensitive to x. A peak in the elastic diffuse scattering is also present at the same q as the kink. Amplitude-contrast electron-microscope images display a "tweed" pattern characteristic of many martensitically transforming materials. The high-resolution (phase-contrast) electron image reveals microscopic deviations of the cubic structure and can be viewed as embryos of the low-temperature $(5,\bar{2})$ martensitic phase. The displacement fields associated with these distortions are shown to be the origin of the elastic central peak observed in the experiments. Temperature-dependence studies show a substantial softening of the phonon branch in the vicinity of the kink and the elastic diffuse scattering increases as T approaches T_M, the martensitic-transformation onset temperature. The mode never becomes completely soft. Furthermore, the softening is narrowly restricted to the $[\bar{1}10]$ direction, which is perpendicular to [110]. Studies of the phonon dispersion curve under uniaxial stress show a softening of the phonon mode near the q value of the kink, which can be interpreted in terms of Clapp's proposed localized-soft-mode theory of nucleation of materials undergoing martensitic transformation.

I. INTRODUCTION

The study of martensitic transformations (MT's) have interested metallurgists for nearly a century.[1] The use of MT's in physical metallurgy has been prominent in the development of alloys with high strength (e.g., steels) and others with exotic properties (e.g., shape-memory alloys). Various applications of MT's have evolved, despite incomplete understanding of the mechanism. Metallurgists have a precise, albeit phenomenological, definition of MT's, whereas physicists have come to use the term loosely to define many first-order phase transitions with acoustic anomalies. It is generally agreed by both disciplines, however, that MT's are first-order, displacive (meaning a coordinated displacement of atoms over distances much less than the atomic spacing), and diffusionless (meaning no atom by atom jumping within the cell as in order-disorder transitions).[2] Shear strains are known to play an important role. Furthermore, nucleation and growth is important because of the first-order nature of the transformation; the system passes through a two-phase regime with distinct interfaces between the two phases. The role of atomic displacements in the nucleation process is still not completely understood.[1-3]

In this paper we describe the study of one system, Ni-Al, over a range of compositions with the aim at understanding the role of the atomic displacements in the MT of the ordered phase. The crystal structure of the high-temperature or parent β_2 phase is cubic B2 or CsCl type [space group O_h^1 $(Pm3m)$]. It is stable over the composition interval 38–68 at. % Ni at elevated temperatures and approximately 45–60 at. % at room temperature.[4] The focus of this report is on the Ni-rich β_2 phase where the excess Ni atoms in the off-stoichiometric alloys are randomly substituted on the Al sublattice as shown in Fig. 1(a). For compositions in the 60–68 at. % Ni range, a reversible martensitic transformation is known to occur at low temperatures when the β_2-phase material is rapidly quenched to avoid thermally activated decomposition.[5] It is well established that the high-temperature parent phase is cubic, but the low-temperature product structure varies with composition.[5] A plot of the transformation temperature T_M (M_S is used in the metallurgical literature[1]) as a function of composition x is given in Fig. 1(b).[5,6] The striking feature of Fig. 1(b) is the extreme sensitivity of the T_M to composition. A change of as little as 1 at. % can change T_M by as much as 100 K. The origin of this strong composition dependence is an interesting scientific problem, but there is also a practical problem: In experimental studies of these alloys, the compositions (including impurities) must be carefully controlled.

We have employed diffuse neutron diffraction and inelastic scattering, electron diffraction, and imaging procedures using samples from the same alloy ingots. We show that there are indeed anomalous atomic displacements in the quenched β_2 phase as evidenced by diffuse scattering observed in the neutron-scattering experiments and with the electron microscope. We also demonstrate that the phonon-dispersion curves exhibit strong, unique anomalies in a particular phonon branch away from the zone center. These anomalies may be interpreted as precursors of the low-temperature martensitic phase.

II. EXPERIMENT

A. Ni_xAl_{100-x} samples

Several different compositions were studied with $x=50$, 58, 62.5 and 63.9 at. % as determined by wet chemical analysis. The crystals were of various shapes and sizes, and the $x=50$ and 58 at. % samples were used in an earlier x-ray study.[7] Of the four samples, only the two with the highest composition exhibited a MT; their transition temperatures are shown in Fig. 1(b). We can see that T_M measured falls within the wide range delineated by various other studies.[5,6] By far, our most extensive experimental work was performed on the $x=62.5$ alloy. This crystal was grown especially for this series of experiments at the United Technologies Research Center. It was carefully heat treated in order to reduce any compositional inhomogeneities. The sample for the neutron scattering was cut from a large boule and was cubic in shape ($5\times5\times5$ mm^3) with each face parallel to a (100) plane. Smaller samples for the electron-microscopy studies were prepared from the same boule.[8–10] The $x=62.5$ crystal was of exceptionally high quality, with a mosaic of less than 6 min. The room-temperature lattice parameter was $a_0=2.858$ Å.

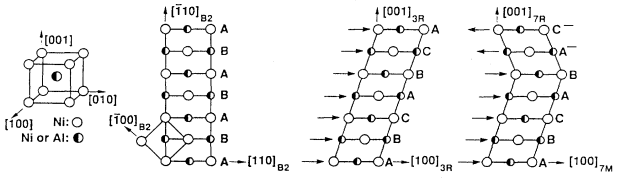

(a)

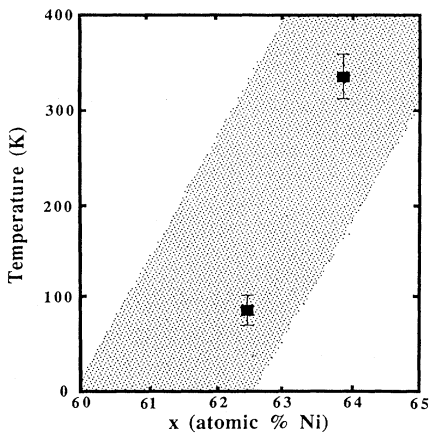

(b)

FIG. 1. (a) Crystal structure, as viewed along [001] direction, of the close-packed planar stacking sequences of the high-temperature cubic (parent) phase and low-temperature martensite (product) phase of Ni_xAl_{100-x}. From left to right: the Ni-rich β_2 cubic structure; the $AB\ldots$ stacking of (110) planes in the β_2 phase; the $ABC\ldots$ stacking of $(110)_{\text{cubic}}$ planes in $3R$ martensite (for $63<x<68$ at. % Ni; the $ABCABA^-C^-\ldots$ stacking of $7M$ $(5,\bar{2})$ martensite (for $60<x<63$ at. % Ni). See Ref. 1 for explanation of the product-phase stacking notations. (b) Measured values of T_M for the two transforming Ni-Al alloys studied here. The points fall within the wide range of values (shaded band) obtained in various investigations; for a review see Ref. 6. The steep slope of the band and its breadth clearly indicate the sensitivity of T_M to alloy composition.

B. Neutron scattering

Most of the experiments were performed at the High Flux Beam Reactor at Brookhaven National Laboratory. The measurements on $x=58$, however, were performed at the Orphée reactor at the Laboratoire Léon Brillouin, Saclay, France. The majority of the data were collected with a fixed final energy of $E_f=14.7$ or 30.5 meV. Pyrolytic graphite [PG (0002)] reflections were used for monochromator and analyzer. A PG filter was also used after the sample to eliminate higher-order contamination. Collimations were chosen depending upon the conflicting needs of intensity and resolution.

Care was taken to mount the samples as stress free as possible. They were usually wrapped in aluminum foil and the foil glued to a support. This was placed in an aluminum can which was filled with an atmosphere of He gas. The can, in turn, was placed onto the cold stage of an Air Products Displex refrigerator. The temperature could be regulated from 10 to 350 K to within 0.1 K.

C. Electron microscopy

Conventional electron microimages (amplitude contrast) and selected-area electron-diffraction (SAED) patterns were obtained with the standard JEOL 200 CX instrument equipped with double-tilt heating and cooling stages at Lawrence Livermore National Laboratory. High-resolution imaging (phase contrast), which is limited to room temperature, was carried out on the JEOL top-entry 200 CX and ARM instruments at the National Center for Electron Microscopy at the Lawrence Berkeley Laboratory.

III. NEUTRON SCATTERING

A. Composition dependence of phonons

Phonon-dispersion curves were determined from inelastic scattering along four high-symmetry directions: $[\zeta00]$, $[\zeta\zeta0]$, $[\zeta\zeta\zeta]$, and $[2\zeta\,\zeta\,\zeta]$ in the $x=62.5$ sample. The results are shown in Fig. 2. Measurements were also

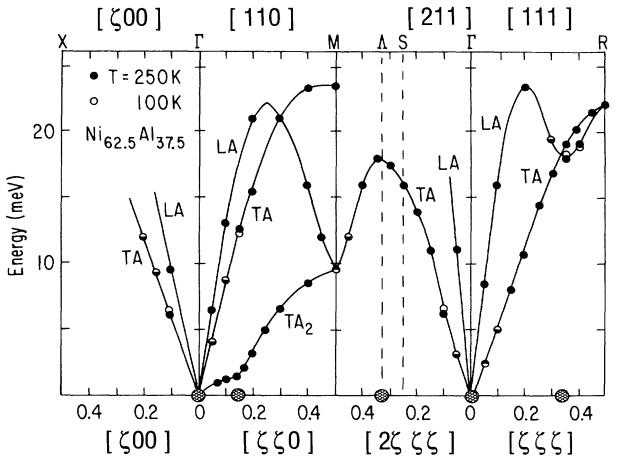

FIG. 2. Measured acoustic-phonon dispersion curves for $Ni_{62.5}Al_{37.5}$ at $T=250$ and 100 K. The shaded circles at $E=0$ correspond to elastic diffuse scattering.

made along the first three directions in $x=58$. Most branches behave normally except for the transverse mode propagating along the $[\zeta\zeta 0]$ direction and the longitudinal mode propagating along $[\zeta\zeta\zeta]$. The dispersion curves of the branches are independent of composition except for the unusually low-energy $[\zeta\zeta 0]$-TA_2 or Σ_4 branch. This TA_2 branch exhibits an anomalous kink, or dip, in all compositions studied. The displacements of the atoms for this transverse mode propagating in the $\langle 110\rangle$ direction are along the perpendicular direction $\langle 1\bar{1}0\rangle$. For the limit $q\rightarrow 0$ this corresponds to the elastic constant $C'=\frac{1}{2}(C_{11}-C_{12})$ and is related to sliding of $\{110\}$ planes along $\langle 1\bar{1}0\rangle$ directions. In most pure metals and solid solutions with bcc or CsCl-type structures, C' is anomalously low and uniquely related to the martensitic transformations.[11]

The anomalous feature observed in the $[\zeta\zeta\zeta]$-LA branch is the dip at $\zeta=\frac{1}{3}$ or $\frac{2}{3}$ of the zone bounday. All bcc metals show a dip at this wave vector due to the Coulomb contribution of a bcc arrangement of positive ions to the dynamical matrix. In some metals, such as Zr,[12] Ti,[13] and Nb,[14] the dip is enhanced by electron-phonon coupling. This dip is relevant to the formation of an ω phase (a hexagonal or trigonal structure that is only fully stable at high pressures[15]) because it is just the displacements of this mode that are needed to obtain its structure.[16]

The hatched regions along the abscissa in Fig. 2 indicate the presence of elastic diffuse scattering. The temperature dependence of the diffuse scattering that is situated at Bragg peaks and near $\frac{1}{6}[110]$ are related to the MT. These relations are discussed in detail below. The elastic diffuse scattering found at $\frac{1}{3}[111]$ (which is equivalent to $\frac{1}{3}[211]$) has the same form as ω-phase scattering observed in bcc or CsCl-type solid solutions such as Zr-Nb,[17] Ti-Mo,[18] and NiTi.[19] This effect was studied in the NiAl β_2 phase as a function of composition by x-ray diffraction.[7] It was shown that the intensity of the diffuse scattering increases as Ni content deviates to either side of $x=0.5$. In the present experiments we observed that the diffuse scattering is temperature independent as are the phonon energies in the region $\frac{1}{3}[111]$. However, the elastic diffuse scattering, as well as transmission-electron-microscopy (TEM) observations, indicate that ω-like distortions are present in the as-quenched material, but a transformation to the ω-related metastable Ni_2Al phase never occurs with rapid cooling. On the other hand, Ni_2Al will form when the alloy is heat treated at temperatures well above room temperature

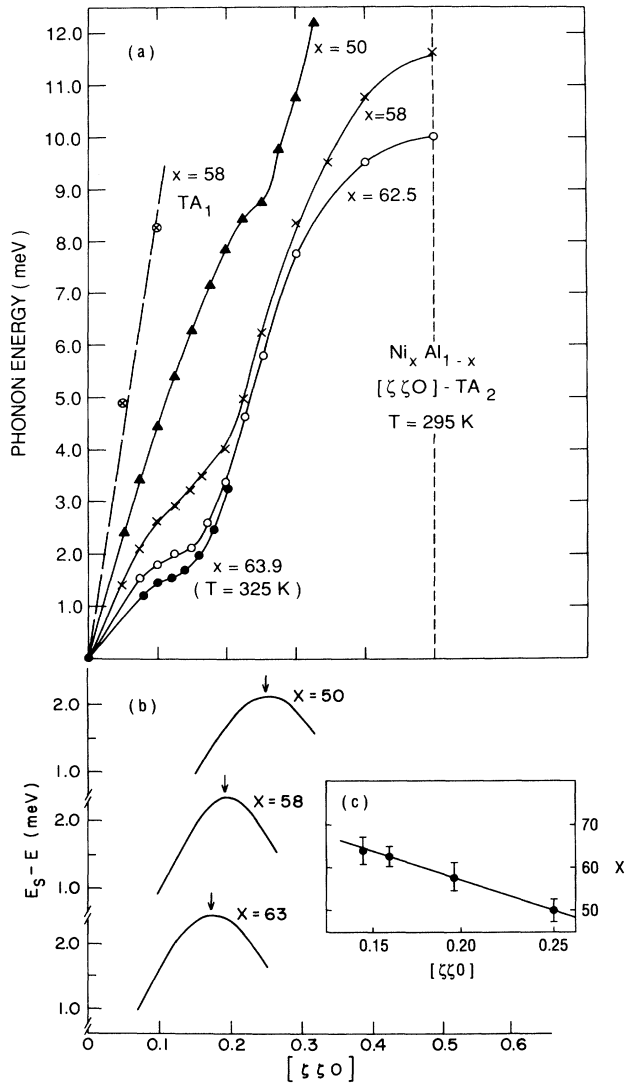

FIG. 3. (a) Dispersion curves of the [110]-TA_2 branch for Ni_xAl_{100-x} for $x=50$, 58, 62.5, and 63.9 at.%. The TA_1 branch for $x=58$ is also shown. (b) Deviation of the measured phonon energy E from that determined by assuming a sine-wave dispersion E_s. (c) Variation of the maxima of E_s-E with composition x.

(i.e., well above T_M).[20,21] In summary, these ω-like effects play no role in the MT studied here.

Figure 3(a) shows the dispersion curve for the [$\zeta\zeta$0]-TA_2 branch for the four compositions studied. It is readily apparent that as x increases the entire branch softens. This is in accord with ultrasonic measurements of the elastic constants for several different compositions.[22] The elastic constants determined from the initial slope of the dispersion curve are in good agreement with the ultrasonic studies. The severe elastic anisotropy is also apparent in this figure since the TA_1 mode for $x=58$ is also shown. The polarization for this branch is along [001] and corresponds to the elastic constant C_{44} for $q\rightarrow 0$. The elastic anisotropy factor is $A=C_{44}/C'$, and A increases dramatically with x since C_{44} is essentially composition independent. For example, from the recent work by Zhou, Cornely, and Trivisonno,[23] A is 22.8, 24.8, and 34 for $x=62$, 62.5, and 63, respectively. The most unusual feature is the "wiggle" or "kink" in each dispersion curve.[24] The kink gets more pronounced and its position decreases as x increases. To determine the concentration dependence of the value in the anomalous region, we calculated the deviation of the measured phonon energy E from that determined by assuming $E_s \propto v_s \sin\pi\zeta$, where v_s is the velocity of sound. In Fig. 3(b) we plot $E_s - E$ vs x. The maxima correspond to the largest deviation, which shifts linearly with x as shown in Fig. 3(c).

B. Temperature dependence

The only phonon branch for $x=58$, 62.5, and 63.9 that displays any anomalous temperature dependence is the TA_2 branch. For all other branches the phonon energy increases slightly with cooling, as expected for normal anharmonic processes. The temperature dependence of the energy of several phonons is shown in Fig. 4 for $x=58$. This composition does not undergo a MT for $T>12$ K. The major temperature dependence is restricted to the region of the phonon anomaly, namely, $\zeta\sim 0.2$. For ζ smaller and larger than this value, there is a comparatively smaller temperature variation. Measurements of diffuse scattering about the allowed Bragg peaks revealed some additional intensity, but it was nearly independent of temperature.

The temperature dependence of this TA_2 branch for $x=62.5$ and 63.9, compositions that undergo a MT, exhibits remarkable, though incomplete, softening. Let us first discuss the $x=62.5$ sample.[25] Figure 5 shows the inelastic spectra measured at $\zeta=0.16$, near the region of the kink in the dispersion curve. It is readily seen that between room temperature and just above $T_M=80$ K, the phonon energy varies by nearly a factor of 2. An intense elastic central peak develops as T_M is approached. The temperature-dependent behavior is summarized in Fig. 6. Figure 6(a) shows the low-energy part of the [$\zeta\zeta$0]-TA_2 phonon-dispersion curve, measured at several different temperatures. The phonon energy develops a clear minimum around $\zeta=\frac{1}{6}$ as $T\rightarrow T_M$. Figure 6(b) shows the elastic scattering measured along the same [$\zeta\zeta$0] direc-

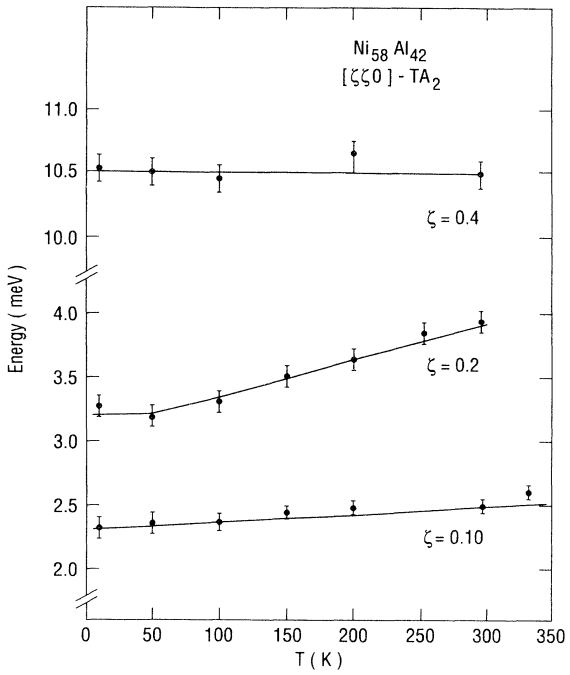

FIG. 4. Temperature dependence of three phonons of the [$\zeta\zeta$0] branch measured at $\zeta=0.1$, 0.2, and 0.3 for the $Ni_{58}Al_{42}$ alloy.

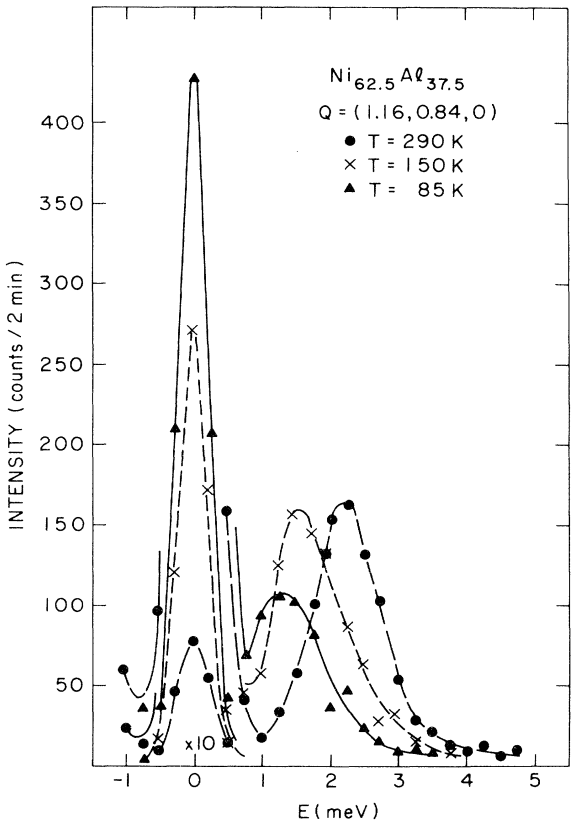

FIG. 5. Inelastic-neutron-scattering ($x=62.5$) spectra for the [$\zeta\zeta$0]-TA_2, $\zeta=0.16$ phonon measured at several temperatures in the cubic phase. For this alloy $T_M=80$ K.

tion. An elastic central peak develops at the same $\zeta=\frac{1}{6}$ as the minimum of the dispersion curve. In addition to this peak in the elastic scattering, there is intense diffuse scattering that diverges as $\zeta\rightarrow 0$. This is more clearly seen in Fig. 7, which shows equi-intensity contours of the elastic scattering measured about the (1,1,0) Bragg peak. The scattering is a ridge or streak emanating from the [110] Brillouin-zone center with a maximum superimposed at $\zeta\approx\frac{1}{6}$. It will be shown in Sec. IV that similar features are seen in the SAED patterns measured on thin sections of the same material. It is important to note that electron diffraction cannot distinguish between phonons giving rise to thermal diffuse scattering and a static response. The neutron scattering can and shows that the diffuse scattering is indeed elastic, since its energy width is limited by the instrumental resolution.[26] Both the pho-

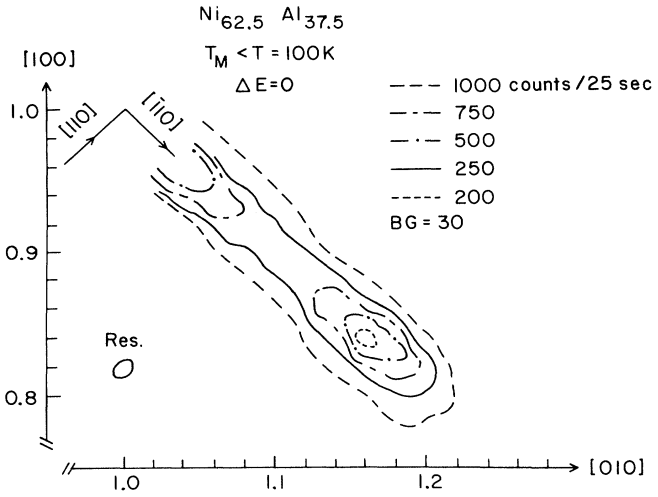

FIG. 7. Equi-intensity contours of the elastic diffuse scattering measured about the (1,1,0) Bragg peak for $x=62.5$ alloy.

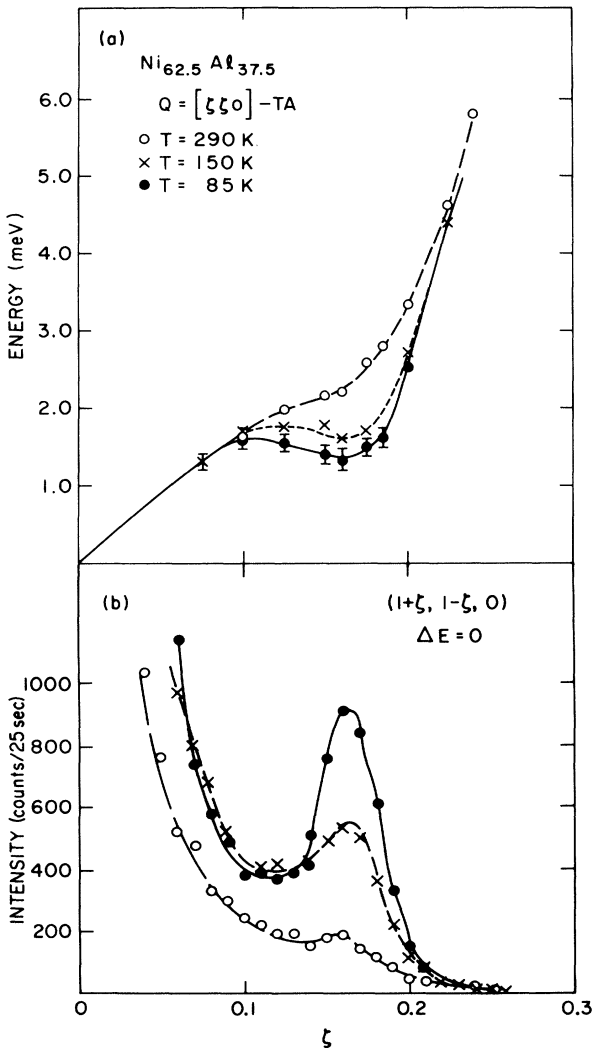

FIG. 6. (a) Temperature dependence of the dispersion curve of the $[\zeta\zeta 0]$-TA_2 mode for $x=62.5$. (b) Temperature dependence of the elastic scattering along the $[\zeta\zeta 0]$-TA_2 direction.

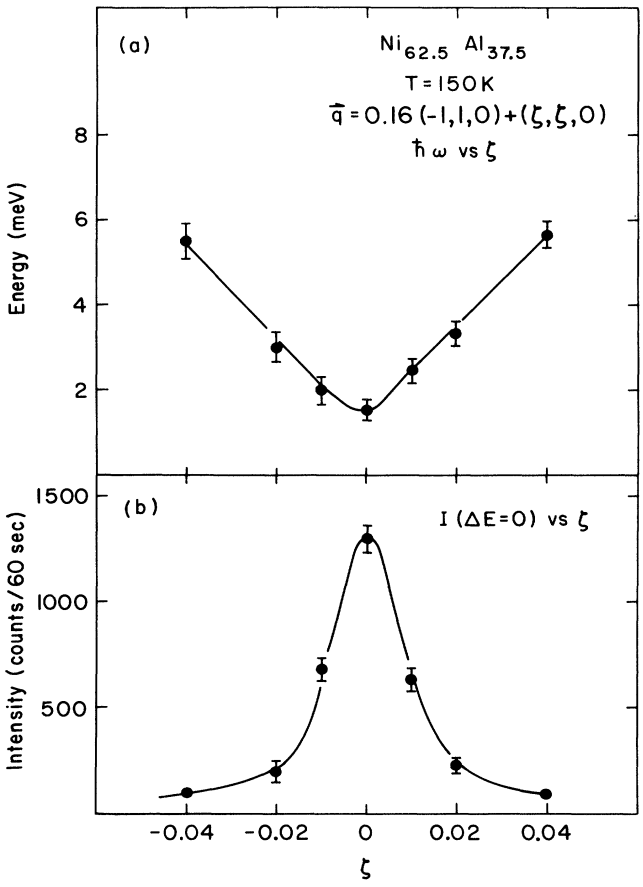

FIG. 8. (a) Phonon energy measured along a perpendicular $[\bar{\zeta}\zeta 0]$ direction from the $\mathbf{q}=0.16(1,1,0)$ point where the dispersion curve is a minimum. (b) The dependence of the elastic intensity along $[\bar{\zeta}\zeta 0]$ from $\mathbf{q}=0.16(1,1,0)$.

non energies and elastic scattering were measured perpendicular to the [$\bar{1}$10] ridge of diffuse scattering. Figure 8(a) shows a plot of the phonon energy measured along the [110] direction from the 0.16 ($\bar{1}$10) point where the phonon energy is a minimum and the elastic central-peak intensity is a maximum. The phonon energy increases dramatically and the central peak intensity decreases even more dramatically as ζ deviates from the [110] direction. This demonstrates that the anomalies in both the phonon-dispersion curve and diffuse scattering are restricted to a narrow region or valley along the [$\bar{1}$10] direction.

Figure 9 gives a summary of the temperature dependence of the "softening" of the phonon and central-peak intensity. Figure 9(a) is a plot of $(\hbar\omega)^2$, and Fig. 9(b) is the reciprocal of the elastic intensity versus temperature, both measured at $q=0.16$[110]. The square of the phonon energy follows a linear curve and extrapolates to zero at $T_E=-30$ K. I^{-1} shows a minimum near 80 K, which is T_M measured on cooling. Both curves show an increase below T_M, the start of the mixed-phase regime where the volume fraction of the parent cubic phase starts to decrease with cooling. I^{-1} above T_M is not linear and varies nearly quadratically with temperature.

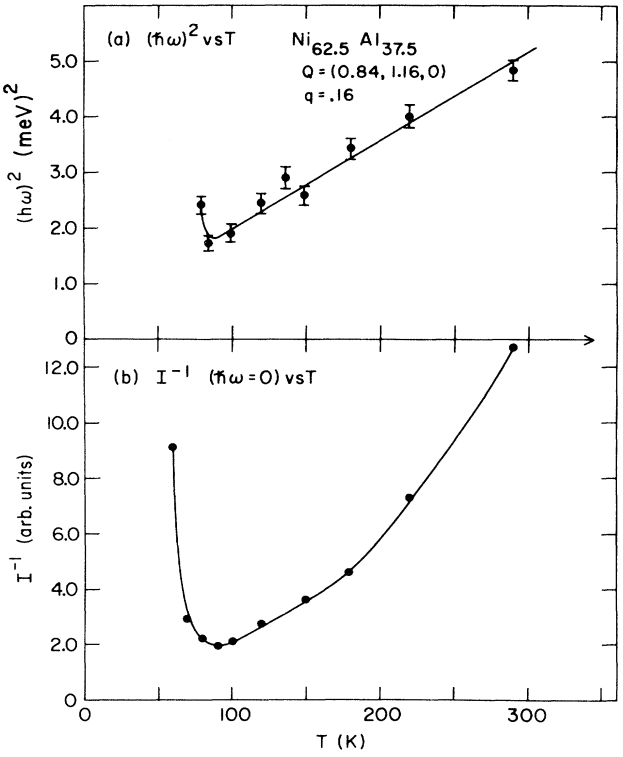

FIG. 9. (a) $(\hbar\omega)^2$ vs T for the [$\zeta\zeta$0]-TA$_2$ mode for $\zeta=0.16$ (b) I^{-1} ($\hbar\omega=0$) vs T for the elastic scattering along the [$\zeta\zeta$0]-TA$_2$ direction for $\zeta=0.16$. The upturn at low temperatures indicates that the crystal has partially transformed.

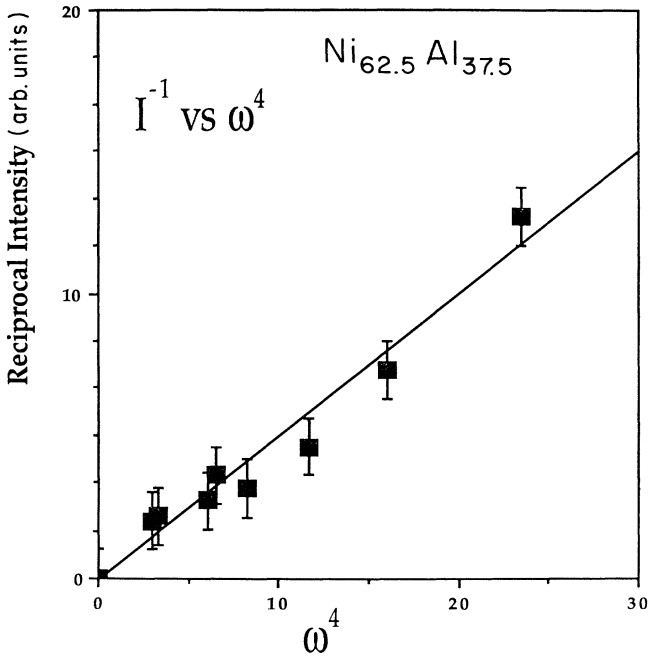

FIG. 10. Reciprocal of the intensity of the elastic central peak measured at $\zeta=0.16$ vs $(\hbar\omega)^4$ of the phonon measured at the same ζ.

This is borne out in Fig. 10 where $(\hbar\omega)^4$ is plotted versus I^{-1}. The linear relation between these two quantities is apparent. The importance of this relation in determining the origin of the elastic diffuse scattering is discussed below.

The diffuse scattering and low-energy phonon behavior were also studied in the $x=63.9$ alloy. The elastic diffuse scattering measured along the [$\bar{\zeta}\zeta$0] direction about the (1,1,0) Bragg peak is shown in Fig. 11 and com-

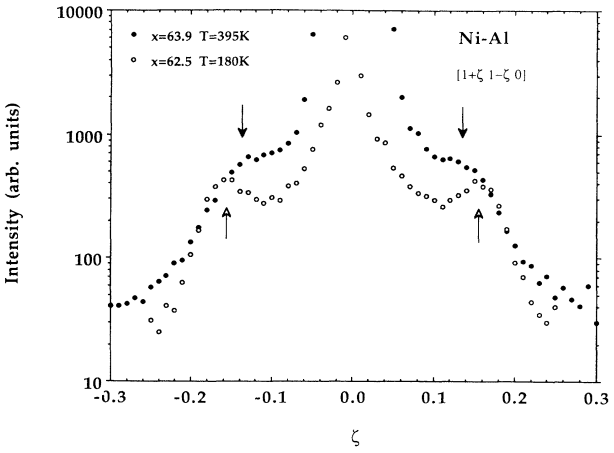

FIG. 11. Elastic diffuse intensity measured transverse to the Q=(1,1,0) Bragg peak for the (●). $x=63.9$ at. % at $T=395$ K ($T-T_M=55$ K) and (○) $x=62.5$ at. % at $T=180$ K ($T-T_M=100$ K).

pared with the measurements on the $x=62.5$ alloy. For this alloy the MT temperature is $T_M \sim 330$ K as determined by the onset of the large increase in the diffuse scattering. Even though the measurement of Fig. 11 was performed at a temperature closer to T_M [$(T-T_M)=55$ K] than the $x=62.5$ sample [$(T-T_M)=100$ K], the satellite peaks are much broader and not clearly resolved. There also seems to be more of the monotonic diffuse scattering, which diverges at $\zeta=0$. The position of the satellites ($\zeta \sim 0.14$) is closer to the Bragg peak than in the $x=62.5$ sample. The temperature dependence of the low-energy portion of the phonon-dispersion curve is shown in Fig. 12. At high temperatures there is a well-defined kink, and it, too, gets more pronounced as T approaches T_M. The anomaly or kink in the dispersion curve is at a smaller wave vector than for $x=62.5$ (see Fig. 3). Furthermore, the anomaly does not deepen as much with temperature as it does in the $x=62.5$ sample (cf. Figs. 3 and 12). The shallowness of this anomaly is undoubtedly related to the breadth of the elastic satellites. The temperature dependence of the phonon energy is summarized in Fig. 13, where the square of the phonon energy is plotted as a function of temperature. For comparison the results for $x=62.5$ are also plotted. The curves are linear and approximately parallel. For the $x=63.9$ sample the energy extrapolates to zero near 100 K, whereas for $x=62.5$ the extrapolation is to -30 K.

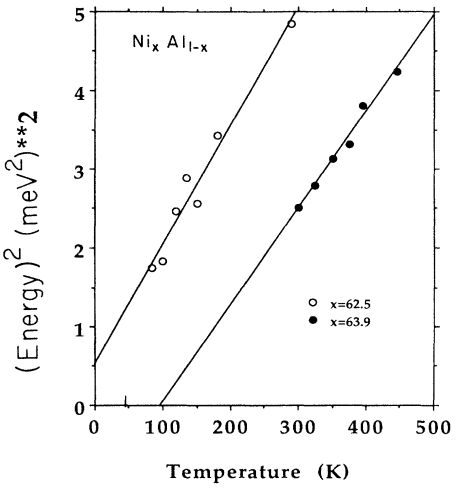

FIG. 13. $(\hbar\omega)^2$ vs temperature for the mode measured at $\zeta=0.16$ for $x=62.5$ (●) and at $\zeta=0.14$ for $x=63.9$ (○).

C. Stress dependence

Stress is known to play a critical role in martensitic transformations.[9,27,28] In fact, the $7M$ structure of the low-temperature phase of $Ni_{63}Al_{37}$ was first discovered by inducing the martensite phase at room temperature under tensile loading[29,30] [the long-period structure is shown schematically on the right in Fig. 1(a)]. Also, in recent high-resolution electron-microscopy studies near a crack[9] in $Ni_{62.5}Al_{27.5}$, the structure in the highly stressed region ahead of the crack corresponded to the $7M$ structure. It is of extreme interest to probe the lattice dynamics, especially the mode-softening features, as a function of stress because it will help elucidate the displacive transformation mechanism. We constructed a simple C-clamp device where, by means of a screw, we could apply a uniaxial compressive stress along the [001] direction and study the behavior of the [110]-TA_2 branch at room temperature. Figure 14 shows the stressed and unstressed behavior of the low-energy portion the [110]-TA_2 phonon. It is clear that the phonon energy decreased with applied stress. Simultaneously, the elastic diffuse scattering increased and the satellite peaks shifted slightly to *larger*

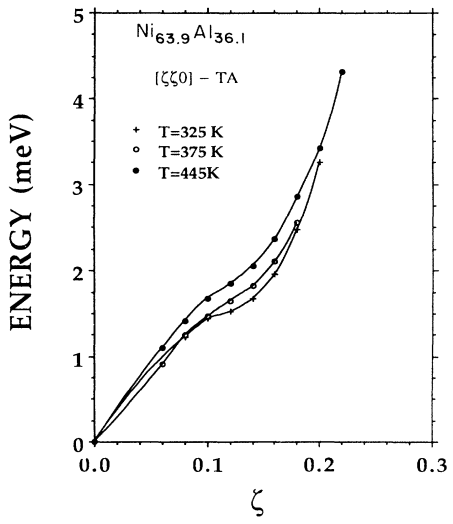

FIG. 12. Temperature dependence of the low-frequency part of the dispersion curve of the [$\zeta\zeta$0]-TA_2 branch for the $x=63.9$ at. % alloy. $T_M=345$ K.

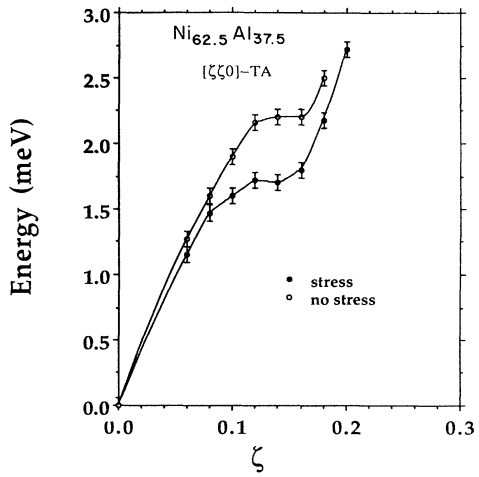

FIG. 14. Effect of unixial stress applied along [001] on the low-energy portion of the [$\zeta\zeta$0]-TA_2 branch for $x=62.5$.

wave vectors. The latter was also observed with electron scattering as well as imaging in the elastically stressed parent phase adjacent to the product martensite in the crack process zone (see Fig. 6 in Ref. 9). Detailed accounts of these stress and temperature-dependent effects are planned to be presented in separate publications.

IV. ELECTRON MICROSCOPY AND DIFFRACTION

The electron-microscopy methods and observations have been discussed in detail elsewhere.[8-10] We shall summarize the salient features. Figure 15(a) shows the electron-diffraction pattern of the as-quenched $Ni_{62.5}Al_{37.5}$ alloy. Clearly seen are streaks along the $\langle \zeta\zeta 0 \rangle$ directions emanating from each of the Bragg peaks. Densitometer traces [Fig. 15(b)] of one of these streaks reveal a broad maximum or satellite centered at $\zeta \sim 0.16$, which becomes more pronounced as T decreases. These peaks are superimposed upon diffuse streaking that falls off monotonically with ζ and also increases in intensity as T is lowered. The two-beam, bright-field image formed from a (2,0,0) Bragg reflection plus diffuse scattering is shown in Fig. 15(c). Clearly seen is the characteristic "tweed" observed in many systems undergoing MT's.[21,31] It is evident as diffuse striations parallel to $\{1,1,0\}$ planes with a spacing of $\sim 5-10$ nm. Just as the diffuse-streaking intensity increases upon cooling, so does the tweed amplitude, and the striations become more sharply defined and regular as T decreases.

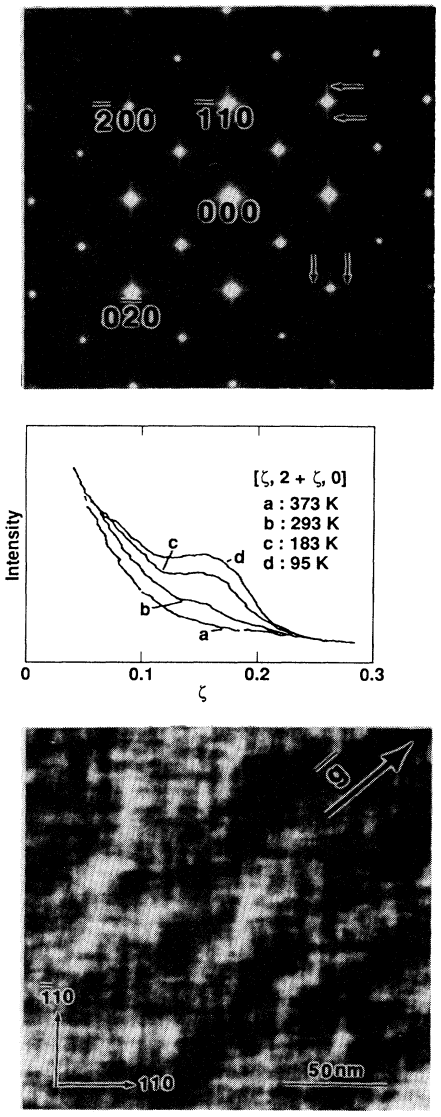

FIG. 15. Electron-microscopy and -diffraction observations of the premartensitic microstructure of β_2 in $Ni_{62.5}Al_{37.5}$: (a) Symmetric (001) zone-axis diffraction pattern obtained at 293 K; arrows indicate positions of satellites superimposed on the $\langle \zeta\zeta 0 \rangle$ diffuse streak. (b) Densitometer traces along $[\zeta\zeta 0]$ of the diffuse scattering for different temperatures T as $T \rightarrow T_M$. (c) Two-beam bright-field image, (001) orientation showing tweed strain contrast (see Refs. 8–10 for complete details).

The high-resolution multibeam phase-contrast imaging mode was used to observe the local atomic configurations giving rise to the streaking in the diffraction pattern. Since an undistorted $B2$ lattice image can not be obtained experimentally, it was calculated using appropriate choices of imaging parameters.[8] The result [Fig. 16(a)] reveals a square pattern of white dots corresponding to the projected columns of atoms of either pure Ni or the randomly mixed Ni and Al sublattice sites. The high-resolution image of the as-quenched sample [Fig. 16(b)] shows considerable local deviation from the ideal lattice-dot pattern. A series of diffuse bands with spacing of approximately 1.3 nm roughly parallel to (110) and $(\bar{1}10)$ planes are shown. This is the reciprocal of the periodicity of the satellite peaks observed in reciprocal space at 0.16 in the electron-diffraction pattern [Fig. 15(b)] and more clearly in the elastic neutron scattering discussed earlier.

V. DISCUSSION

Most of the phonon branches show only a small change in frequency with composition and temperature. Hallman and Svensson[32] recently performed a lattice dynamical study of Ni_xAl_{100-x} for $x = 50$ and 58 at. %. Their results for $x = 50$ are in agreement with the independent study of Mostoller *et al.*[33] They also studied the optic modes in these two alloys and showed that they were also very composition dependent. They performed a Born–von Karmen analysis of the phonon-dispersion curves using fifth-neighbor force constants. The largest force constants were for the first and second neighbors, and the biggest change (35%) as a function of composition occurred for the second-neighbor force constants.

The only transverse-acoustic branch that shows any composition and temperature dependence is the $[\zeta\zeta 0]$-TA_2 mode. As noted earlier, this branch has long been recognized to play a major role in the stability of bcc lattices. The slope of the $q \approx 0$ regime corresponds to the elastic constant $C' = \frac{1}{2}(C_{11} - C_{12})$. A large elastic anisotropy, defined above as $A = C_{44}/C'$, exists in most β-phase alloys mainly because C' is remarkably small.[1,11]

Zener[34] noted this over 40 years ago and suggested that this low value of C' is a result of the ion-exchange interaction which renders the bcc lattice mechanically unstable with respect to a shear propagating along [110] direction and displacement along $[\bar{1}10]$. The small value of C' indicates that there is a weak coupling between the $\{110\}$ planes and they can easily slide relative to one another. This weak coupling and sliding results in an entire range of possible polytype structures in disordered and ordered bcc-based materials.[1] The stacking sequence of planes can vary along the [110] direction. Some frequently observed structures are the $2H$ and $9R$ forms corresponding to modulations with wavelengths of 2 and 3 times the [110] repeat distance, respectively.[1] Precursors of this structure should appear as anomalies in the $[\zeta\zeta 0]$ phonon branch at values of $\zeta=\frac{1}{2}$ and $\frac{1}{3}$, respectively, and indeed these have been observed.[35]

For $Ni_{62.5}Al_{37.5}$ an anomaly exists at $\frac{1}{6}$ [110], which is viewed as a precursor of the low-temperature structure, which is known to have a $7M$ structure at low temperatures[5,10,30] [see Fig. 1(a)]. This structure corresponds to a sevenfold modulation along the [110] direction with successive $\{110\}$ planes displaced along the $[1\bar{1}0]$ direction. The stacking sequence is called $(5,\bar{2})$, which corresponds

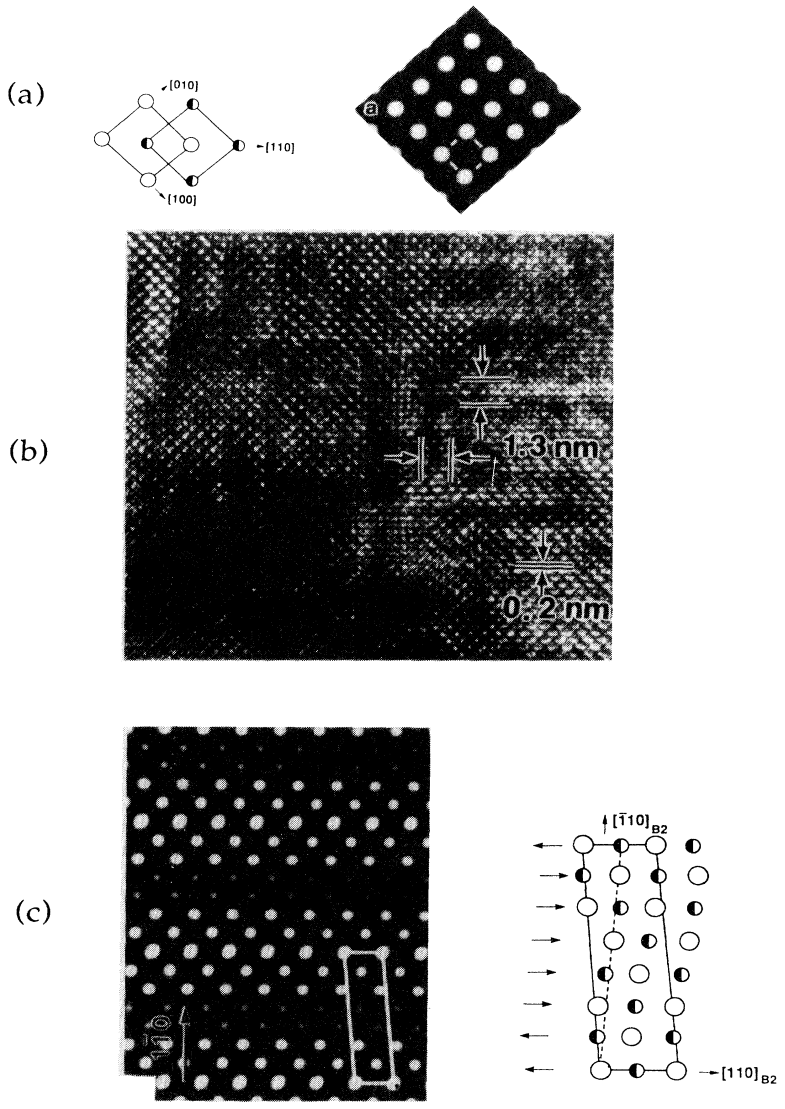

FIG. 16. High-resolution electron microscopy observations of the premartensitic microstructure of β_2 in $Ni_{62.5}Al_{37.5}$ at 293 K: (a) The calculated ideal (001) image, i.e., no local lattice distortion [atomic site notation is the same as in Fig. 1(a)]. (b) The observed image showing local atomic dispacements and a micromodulated domain structure. (c) The $\{110\}$-$\langle 1\bar{1}0\rangle$ shear-plus-shuffle atomic displacement model of the premartensitic micromodulation. The schematic is to the right and the calculated image is to the left (see Refs. 8–10 for complete details).

to five planes displaced along [110] and then two planes displaced in the opposite direction along $[\bar{1}\,\bar{1}0]$ [see Fig. 1(a)]. Very recently, Noda *et al.*[36] refined in more detail the low-temperature phase and found a monoclinic structure with space group $P2/m$. They also pointed out that the displacement of each layer cannot be obtained by "freezing" the pattern of the phonon displacements associated with the anomalous phonon at 0.16[110], but rather the displacement modes are considerably anharmonic. A model based upon the local vibrational mode (site-independent scheme) was applied to understand the transition mechanism.[37]

Alternatively, Gooding and Krumhansl[38] developed a Landau-type theory to describe the transition, which contains an anharmonic coupling between a homogeneous strain and a soft phonon at wave vector $[\zeta\zeta 0]$. Particularly, they proposed that there should be displacements with two independent wave vectors $\zeta_1=\frac{1}{7}$ and $\zeta_2=\frac{2}{7}$. These couple with the homogeneous strain associated with the elastic constant C'. Our results are consistent with their calculations in that an anomaly is seen in the phonon branch at $\zeta=0.16$, which couples to the homogeneous strain. This coupling is evident by the strong temperature dependence of the diffuse scattering at small ζ as well as the phonon central-peak region. No anomaly is observed at ζ_2, but, according to the theory, the effect at ζ_2 would be purely anharmonic and it may be very weak and unobservable. More precisely, the anomaly is observed at $\zeta=0.16$, which is different from $\zeta_1=\frac{1}{7}$. Gooding and Krumhansl[38] argue that if there is a wave-vector dependence of the coefficients in the Landau expansion, the modulation wave vector of the martensite phase can be different from the wave vector of the precursor phonon anomaly.

The $Ni_{63.9}Al_{31.1}$ alloy has an anomaly at a *smaller* wave vector, and it exhibits less temperature dependence than the $x=62.5$ alloy (Figs. 12 and 13). The low-temperature martensite of the 63.9 alloy is established by electron-diffraction studies to be the $3R$-type structure[39] [see schematic in Fig. 1(a)]. This $3R$ structure can be viewed as the same as the $7M$ except that there is no periodic modulation of the stacking along the [110] direction. In other words, only the homogeneous strains determine the low-temperature structure. This is consistent with the observation that the phonon dip near $\zeta=0.14$ is not very deep, and hence the strain energy associated with this q vector is not sufficiently large to induce a modulation in the low-temperature phase.

Associated with the dip in the dispersion curves are elastic streaks and satellites whose intensity increases as $T\rightarrow T_M$. This phenomenon is similar to the ubiquitous central peak observed in many other displacive phase transitions.[40] An example is its presence prior to the transition in Nb_3Sn.[41] The origin of the central peak, however, has been an enigma for some time. In most of the cases where it is observed, the phonon energy becomes so low or the soft mode is so overdamped that it is difficult to distinguish between the phonon and central peak. In Ni-Al β_2 phase, however, the phonon energy never becomes completely soft and the central and phonon peaks can be clearly separated over the entire temperature range studied. The energy linewidth of the central peak is resolution limited, as is the case in most other structural phase transformations. This leads us to suspect that the central peak is defect induced. Although no complete theory is available to explain the central peak, there have been several attempts. The simplest theory was proposed by Axe *et al.*[42] and then extended by Halperin and Varma.[43] In this theory it is assumed that unspecified defects are present and the atoms in the neighborhood of the defects are displaced. These displacement fields are a result of the linear response to a force field $F(r)$ that the defects exert on the undistorted lattice. The amplitude of a defect-induced displacement field can then be written as

$$\langle Q_q \rangle = \frac{F_q}{\omega_q^2} .$$

The diffuse scattering arising from the force field is related to the square of the displacements as in a normal phonon response:

$$I_q \propto |Q_q|^2 = \frac{F_q^2}{\omega_q^4} ,$$

where ω_q is the soft phonon at wave vector q. In the limit of $q\rightarrow 0$, ω_q^2 is proportional to the elastic constant, and this scattering is referred to as Huang diffuse scattering (HDS).[44] This relation is confirmed, as shown in Fig. 10, where I^{-1}, the reciprocal of the central-peak intensity at $\mathbf{q}=0.16(1,1,0)$, is plotted as a function of the fourth power of the soft-mode frequency. Thus the defect mechanism for the central peak is confirmed in the Ni-Al β_2 phase.

However, we can go an important step further which will move us closer to an understanding of martensite nucleation. In contrast to most other systems where the central peak is observed, we have obtained an actual picture of the displacement fields giving rise to this scattering. This is achieved by conventional and high-resolution electron microscopy where the diffuse scattering has been imaged as shown in Figs. 15 and 16. The normal (strain-free) simple periodic arrangement of atoms in the cubic phase [Fig. 16(a)] is significantly perturbed, and a mosaic assembly of contiguous domains of 4–6 nm in diameter is apparent. Within the domains is a micromodulated structure, which appears as diffuse bands parallel to (110) and $(\bar{1}10)$ planes. This structure can be simulated in terms of the product $7M$-phase configuration [Fig. 1(a)]. The model assumes a coupling of a $q=0$ homogeneous shear of $(1\bar{1}0)$ cubic planes along [110] directions by a fraction of the total strain necessary to form the $7M$ structure and a $q\neq 0$ sinusodial modulation of atoms along $[\bar{1}10]$ to give an approximate $(5,\bar{2})$ stacking arrangement. The schematic atomic configuration of our model is shown in Fig. 16(c), as well as a calculation of the image. There is a very close agreement between the observed and simulated structures.

Now including the role of defects (i.e. heterogeneous site coupling), we envision that whenever a defect has at least a resolved component of the double-force tensor $\underline{P}$

of the proper transformation-related symmetry, namely,

$$\underline{P}=P\begin{bmatrix}2 & 0 & 0\\ 0 & -1 & 0\\ 0 & 0 & -1\end{bmatrix},$$

there will be an enhanced strain with the symmetry of the softened elastic shear constant C'. Then, according to Gooding and Krumhansl,[38] a further coupling forces the modulation pattern to follow the strain. This yields localized static displacement fields comprising both effects, and these shear-plus-shuffle fields fall off with distance from the originating defects. The composite configurations, called "inhomogeneously strained domains" (ISD's), make up the mosaic assemblies that are seen in the electron microimages of Figs. 15 and 16. The ISD's are similar to the "dressed embryos" that Yamada *et al.*[45] describe in their fluctuation-based "modulated lattice relaxation" model. They were the first to make use of the coupling of modulated and homogeneous strains to develop local pretransformation structure,[45,46] but their treatment did not include an interaction with preexisting defect-displacement fields.

In conclusion, the generalized microstructure evidenced by the HDS and electron-microscope images may be viewed as an array of coherent-strain embryos of the product phase embedded within the parent phase. It is extremely important to note that these particular ISD's, or embryos, are related to the *weakest*, though rather numerous, strain centers that perturb the parent lattice (viz., point defects, impurities, misplaced solute atoms, etc.). Weak strain centers are *not* very potent nucleation sites.[47] However, the same coupling mechanism applies to all other possible defects, such as dislocation tangles, inclusion interfaces, grain boundaries, grain corners, and the surface.[47] These defects, while far fewer in number, have substantially higher associated strains, and heterogeneous nucleation site potency scales with the strain amplitude.[48]

The precise nature of the strain fields of these embryos is still under investigation, but our observations serve as a basis for defining the relationship between the anomalous atomic displacements and nucleation. The idea originated with Clapp's[27] "localized-soft-mode" theory and has been developed further by Guénin and Gobin[28,48] and Guénin and Clapp.[49] In the majority of materials exhibiting MT's, there is never a mode that becomes completely soft at T_M,[50] but it is well known that certain elastic constants are very sensitive to homogeneous stresses and strains, as well as temperature. In the long-wavelength limit the stress dependence is determined by the third-order elastic constants, which are measured only for a very few materials.[51] We have demonstrated in Fig. 14 that even $q\neq 0$ modes can be affected by a homogeneous stress. It is possible that the elastic constants and/or a particular $q\neq 0$ phonon can become unstable *locally* for a particular combination of stresses at a temperature well above the bulk T_M. That is, around a defect in the parent phase, these stresses will drive the energy of the mode toward zero *locally* so that the inhomogeneously strained region (embryo) becomes unstable. At this point the strain embryo, or ISD, transforms into a martensite nucleus.[28,49,52] The likelihood that this will occur at a particular temperature above T_M (i.e., the heterogeneous-site potency) scales with the amount of stress induced by the defect.[47,48,52] These locally stable nuclei should expand somewhat with cooling in response to the temperature dependence of the lattice softening, but they will not be able to grow freely until there is an undercooling ($T=T_M$) sufficient to provide the driving force necessary to overcome the bulk resistance to propagation.[48] A formal description of the nonclassical heterogeneous nucleation sequence has been developed by Gooding and Tanner[53] and is planned to be published elsewhere.

As a final point, we comment on the composition dependence of C' and the origin of the kink in the [110]-TA_2 branch. While the origin of the kink is not fully understood, it is reasonable to look for electronic effects.[24] A simple picture would define the kink as a Kohn anomaly, whose wave vector is directly related to $2k_F$, which defines the Fermi surface along a given direction in reciprocal space. As the composition changes, the Fermi energy should change and cross the Ni d electronic bands at different values. A difficulty with this type of model was recently imposed by calculations of the band structure for Ni_xAl_{100-x} by Liu *et al.*[54] Their results show that the d bands are localized well below (~ 1 eV) the Fermi level and a small shift in E_F would not appear to significantly change the coupling to the d bands. However, subsequent and more detailed calculations by Zhao and Harmon,[55] where the matrix elements for the electron-phonon interaction have been directly calculated, have confirmed the x dependence of the observed anomaly. It thus appears that the electron-phonon coupling is indeed the origin of the anomalous phonon behavior in Ni_xAl_{100-x} in the β_2 phase.

VI. SUMMARY AND CONCLUSIONS

We have presented a study combining both neutron scattering and electron microscopy in order to probe the premartensitic behavior in the β_2 phase of a well-characterized alloy of Ni-Al. Phonon anomalies are seen in the [$\zeta\zeta 0$]-TA_2 branch, at q away from the zone center, which are composition and temperature dependent. As T_M is approached, the phonon anomalies become more pronounced, and elastic diffuse scattering, a central peak, develops at the same wave vector $\mathbf{q}$ as the phonon anomaly. The electron microscope image of this same diffuse scattering observed in the electron diffraction pattern reveals a deviation of the expected cubic structure, even at temperatures well above T_M. These microscopic distorted regions arise from a coupling of defect-induced strain fields and anomalous phonon softening. Such coupling occurs at a wide spectrum of defect sites and becomes more pronounced as T_M is approached. The greater the local distortions, the more potent a site will be as a center for nucleation of the martensite phase. These results will help resolve the heretofore unsolved problem of nucleation and growth occurring in all martensitic transformations.

ACKNOWLEDGMENTS

The authors acknowledge the many illuminating discussions with R. J. Gooding, R. Gronsky, J. Krumhansl, S. C. Moss, G. Shirane, M. Wüttig, and Y. Yamada. One of us (S.M.S.) would like to thank the hospitality at Laboratoire Léon Brillouin, Saclay, France, where some of this work was performed. In addition, the expert technical assistance with TEM experiments of M. Wall is greatly appreciated. We thank J. B. Cohen and C. M. Wayman for providing us with some crystals and D. Pearson and collaborators of the United Technologies Research Center for producing additional crystals. Various other sample preparation tasks were carried out at the Ames Laboratory of Iowa State University by L. Jones and collaborators. We also thank the National Center for Electron Microscopy at Lawrence Berkeley Laboratory for the use of their facilities. The work at Brookhaven National Laboratory was carried out as part of the U.S.-Japan Cooperative Neutron Scattering Program and was supported by the Division of Materials Sciences, U.S. Department of Energy, under Contract No. DE-AC02-76CH00016. The work at Lawrence Livermore National Laboratory was performed under U.S. Department of Energy Contract No. W-7405-ENG-48.

*Permanent address: The University of Western Ontario, Department of Chemistry, London, Ontario, Canada, N6A 5B7.

†Permanent address: University of Antwerp, RUCA, B2020, Antwerp, Belgium.

[1]Z. Nishiyama, *Martensitic Transformations* (Academic, New York, 1978); M. Ahlers, Prog. Mater. Sci. **30**, 135 (1988).

[2]M. Cohen, G. B. Olson, and P. C. Clapp, in *Proceedings of the International Conference of Martensitic Transformations: ICOMAT 1979* (MIT Press, Cambridge, MA, 1979) p. 1.

[3]L. E. Tanner and M. Wüttig, Mater. Sci. Eng. A **127**, 137 (1990).

[4]M. F. Singleton, J. L. Murray, and P. Nash, in *Binary Alloy Phase Diagrams,* edited by T. B. Massalski (ASM, Metals Park, OH, 1986), p. 140.

[5]S. Chakravorty and C. M. Wayman, Met. Trans. A **7**, 555 (1976); **7**, 569 (1976); K. Enami, S. Nenno, and K. Shimizu, Trans. Jpn. Inst. Met. **14**, 161 (1973); K. Enami, A. Nagasawa, and S. Nenno, Scr. Metall. **12**, 223 (1978).

[6]S. Ochiai and M. Ueno, Jpn. Inst. Met. **52**, 157 (1988).

[7]P. Georgopoulus and J. B. Cohen, Acta Metall. **29**, 1535 (1981).

[8]D. Schryvers and L. E. Tanner, Ultramicroscopy **37**, 241 (1990).

[9]L. E. Tanner, D. Schryvers, and S. M. Shapiro, Mater. Sci. Eng. A **127**, 205 (1990).

[10]L. E. Tanner, A. R. Pelton, G. Van Tendeloo, D. Schryvers, and M. E. Wall, Scr. Metall. **24**, 1731 (1990).

[11]N. Nakanishi, Prog. Mater. Sci. **24**, 143 (1980).

[12]C. Stassis, J. Zaretsky, and N. Wakabayashi, Phys. Rev. Lett. **41**, 1728 (1978).

[13]W. Petry, T. Flottman, A. Heiming, J. Trampenau, M. Alba, and G. Vogl, Phys. Rev. Lett. **61**, 722 (1988); W. Petry, A. Heiming, and J. Trampenau, *Neutron Scattering for Materials Science,* Vol. 166 of MRS Symposium Proceedings (MRS, Pittsburgh, 1990), p. 161.

[14]Y. Nakagawa and A. D. B. Woods, in *Proceedings of the International Conference on Lattice Dynamics,* edited by R. F. Wallis (Pergamon, New York, 1965), p. 39.

[15]S. K. Sikka, Y. K. Vohra, and J. R. Chidambaram, Prog. Mater. Sci. **27**, 245 (1982).

[16]H. E. Cook, Phys. Rev. B **15**, 1477 (1977); D. de Fontaine, Metall. Trans. A **19**, 169 (1988).

[17]S. C. Moss, D. T. Keating, and J. D. Axe, *Phase Transitions—1973,* edited by L. E. Cross (Pergamon, New York, 1973), p. 179.

[18]H. Terauchi, K. Sakaue, and M. Hida, J. Phys. Soc. Jpn. **50**, 3932 (1981).

[19]S. M. Shapiro, Y. Noda, Y. Fujii, and Y. Yamada, Phys. Rev. B **30**, 4314 (1984).

[20]F. Reynaud, J. Appl. Crystallogr. **9**, 263 (1976); Scr. Metall. **11**, 765 (1977).

[21]I. M. Robertson and C. M. Wayman, Philos. Mag. A **48**, 421 (1983); **48**, 443 (1983); **48**, 629 (1983), and references therein.

[22]N. Ruscovic and H. Warlimont, Phys. Status Solidi A **44**, 609 (1977); K. Enami, J. Hasunuma, A. Nagasawa, and S. Nenno, Scr. Metall. **10**, 879 (1976).

[23]J. Zhou, P. Cornely, and J. Trivisonno, in Proceedings of the IEEE Symposium on Ultrasonics, Honolulu, 1990, edited by B. R. McAvoy (IEEE, New York, in press), Vol. 3.

[24]S. M. Shapiro, J. Z. Larese, Y. Noda, S. C. Moss, and L. E. Tanner, Phys. Rev. Lett. **57**, 3199 (1986).

[25]S. M. Shapiro, B. X. Yang, G. Shirane, J. Z. Larese, L. E. Tanner, and S. C. Moss, Phys. Rev. Lett. **62**, 1298 (1990).

[26]A recent study using inelastic scattering of γ rays and the same crystal (W. Yelon, private communication) put an upper limit to the energy linewidth of $<3\ \mu$eV.

[27]P. C. Clapp, Phys. Status Solidi B **57**, 561 (1973); Mater. Sci. Eng. A **127**, 189 (1990).

[28]G. Guénin and P. F. Gobin, Metall. Trans. A **13**, 1127 (1982).

[29]Although 7*R* was initially used to describe the low-temperature structure (Ref. 30), we use the notation 7*M* suggested by Ref. 36, which more accurately relates the monoclinic structure.

[30]V. V. Martynov, K. Enami, L. G. Khandros, S. Nenno, and A. V. Tkachenko, Phys. Met. Metall. **55**(5), 136 (1983); Scr. Metall. **17**, 1167 (1983).

[31]L. E. Tanner, Philos. Mag. **14**, 111 (1966); L. E. Tanner, A. R. Pelton, and R. Gronsky, J. Phys. (Paris) Colloq. **43**, C4-169 (1982).

[32]E. D. Hallman and E. C. Svensson, in *Phonons 89,* edited by S. Hunklinger, W. Ludwig, and G. Weiss (World Scientific, Singapore, 1990), Vol. 2, p. 1108.

[33]M. Mostoller, R. M. Nicklow, D. M. Zehner, S. C. Lui, I. M. Mumdenar, and E. W. Plummer, Phys. Rev. B **40**, 2856 (1990).

[34]C. Zener, Phys. Rev. **71**, 846 (1947).

[35]A. Nagasawa, J. Phys. Soc. Jpn. **40**, 1021 (1976); *Proceedings of the International Conference on Martensitic Transformations (ICOMAT-86)* (Japan Institute of Metals, Sendai, 1986), p. 95.

[36]Y. Noda, S. M. Shapiro, G. Shirane, Y. Yamada, K. Fuchizaki, and L. E. Tanner, Mater. Sci. Forum **56-58**, 299 (1990); Phys. Rev. B **42**, 10 397 (1990).

[37]Y. Yamada, Y. Noda, and K. Fuchizaki, Phys. Rev. B **42**, 10 405 (1990).

[38]R. J. Gooding and J. Krumhansl, Phys. Rev. B **39**, 1535

(1989).
[39]L. E. Tanner (private communication).
[40]A. D. Bruce and R. A. Cowley, *Phase Transitions* (Taylor and Francis, London, 1981).
[41]J. D. Axe and G. Shirane, Phys. Rev. B **8**, 1965 (1973).
[42]J. D. Axe, S. M. Shapiro, G. Shirane, and T. Riste in *Amharmonic Lattice, Structural Transitions, and Melting,* edited by T. Riste (Nordhoff, Leiden, 1974), p. 23.
[43]B. I. Halperin and C. M. Varma, Phys. Rev. B **14**, 4030 (1976).
[44]M. A. Krivoglaz, *Theory of X-Ray and Thermal Neutron Scattering by Real Crystals* (Plenum, New York, 1969); E. Burkel, B. V. Guerard, H. Metzger, J. Peisl, and C. M. E. Zeyen, Z. Phys. B **35**, 227 (1979).
[45]Y. Yamada, Y. Noda, M. Takimoto, and K. Furukawa, J. Phys. Soc. Jpn. **54**, 2940 (1985); Y. Yamada, Y. Noda, and M. Takimoto, Solid State Commun. **55**, 1003 (1985).
[46]K. Fuchizaki, Y. Noda, and Y. Yamada, Phys. Rev. B **39**, 9260 (1989).
[47]T. Saburi and S. Nenno, in *Proceedings of the International Conference on Martensitic Transformations (ICOMAT-86)* (Ref. 35), p. 89.
[48]P. F. Gobin and G. Guénin, *Solid State Phase Transformations in Metals and Alloys* (Editions Physiques, Orsay, 1978), p. 573.
[49]G. Guénin and P. C. Clapp, in *Proceedings of the International Conference on Martensitic Transformations (ICOMAT-86)* (Ref. 35), p. 171.
[50]J. A. Krumhansl and R. J. Gooding, Phys. Rev. B **39**, 3047 (1989).
[51]B. Verlinden and L. Delaey, Metall. Trans. A **19**, 207 (1988).
[52]M. Suezawa and H. E. Cook, Acta Metall. **28**, 423 (1980).
[53]R. J. Gooding and L. E. Tanner (unpublished).
[54]S. C. Lui, J. W. Davenport, E. W. Plummer, D. M. Zehner, and G. W. Fernando, Phys. Rev. B **42**, 1582 (1990).
[55]G. L. Zhao and B. N. Harmon, Bull. Am. Phys. Soc. **35**, 576 (1990); (unpublished).

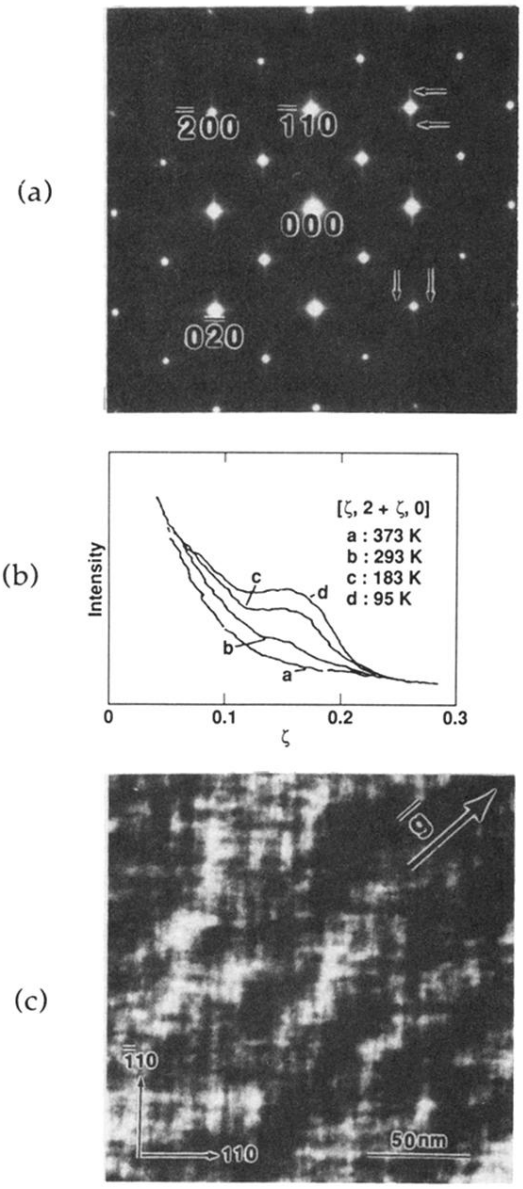

FIG. 15. Electron-microscopy and -diffraction observations of the premartensitic microstructure of β_2 in $Ni_{62.5}Al_{37.5}$: (a) Symmetric (001) zone-axis diffraction pattern obtained at 293 K; arrows indicate positions of satellites superimposed on the $\langle \zeta\zeta 0 \rangle$ diffuse streak. (b) Densitometer traces along $[\zeta\zeta 0]$ of the diffuse scattering for different temperatures T as $T \rightarrow T_M$. (c) Two-beam bright-field image, (001) orientation showing tweed strain contrast (see Refs. 8–10 for complete details).

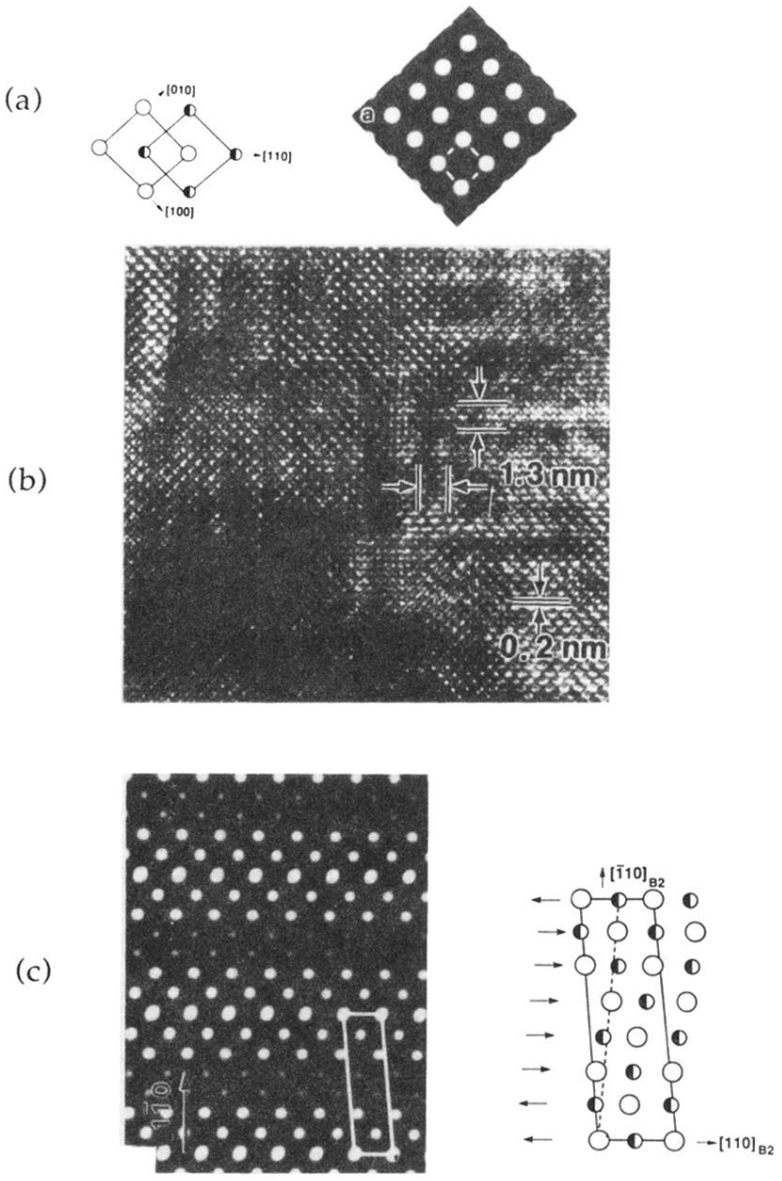

FIG. 16. High-resolution electron microscopy observations of the premartensitic microstructure of β_2 in $Ni_{62.5}Al_{37.5}$ at 293 K: (a) The calculated ideal (001) image, i.e., no local lattice distortion [atomic site notation is the same as in Fig. 1(a)]. (b) The observed image showing local atomic dispacements and a micromodulated domain structure. (c) The $\{110\}$-$\langle 1\bar{1}0\rangle$ shear-plus-shuffle atomic displacement model of the premartensitic micromodulation. The schematic is to the right and the calculated image is to the left (see Refs. 8–10 for complete details).